Substrate Modulus Directs Neural Stem Cell Behavior

Krishanu Saha,* Albert J. Keung,* Elizabeth F. Irwin,† Yang Li,† Lauren Little,* David V. Schaffer,*†‡ and Kevin E. Healy†§

*Department of Chemical Engineering, †Department of Bioengineering, ‡Helen Wills Neuroscience Institute, and §Department of Materials Science and Engineering, University of California at Berkeley, Berkeley, California 94720

ABSTRACT Although biochemical signals that modulate stem cell self-renewal and differentiation were extensively studied, only recently were the mechanical properties of a stem cell's microenvironment shown to regulate its behavior. It would be desirable to have independent control over biochemical and mechanical cues, to analyze their relative and combined effects on stem-cell function. We developed a synthetic, interfacial hydrogel culture system, termed variable moduli interpenetrating polymer networks (vmIPNs), to assess the effects of soluble signals, adhesion ligand presentation, and material moduli from 10–10,000 Pa on adult neural stem-cell (aNSC) behavior. The aNSCs proliferated when cultured in serum-free growth media on peptide-modified vmIPNs with moduli of ≥100 Pa. In serum-free neuronal differentiation media, a peak level of the neuronal marker, β-tubulin III, was observed on vmIPNs of 500 Pa, near the physiological stiffness of brain tissue. Furthermore, under mixed differentiation conditions with serum, softer gels (~100–500 Pa) greatly favored neurons, whereas harder gels (~1,000–10,000 Pa) promoted glial cultures. In contrast, cell spreading, self-renewal, and differentiation were inhibited on substrata with moduli of ~10 Pa. This work demonstrates that the mechanical and biochemical properties of an aNSC microenvironment can be tuned to regulate the self-renewal and differentiation of aNSCs.

INTRODUCTION

The mechanical properties of a cell's environment affect a broad range of its properties, ranging from the morphology of embryonic cells and tissues (1,2), to fibroblast remodeling of collagen extracellular matrices (ECMs) (3,4), to cell motility directed by substrate stiffness (5,6). Recent work also indicated that peripheral nervous system cells (7,8) and PC12 adrenal tumor cells (9,10) show variable neurite extension and branching on mechanically tunable matrices and culture substrates. Substrate and matrix mechanical properties have been implicated in the behavior of tumor cell lines (11) and tumor progression (12). Moreover, the differentiation of epithelial cells (12), myotubes (13), and adult mesenchymal stem cells (14,15) toward particular lineages can be directed by substrate and matrix mechanical properties. These results indicate that cells in general and stem cells in particular are sensitive to the mechanical properties of a surrounding or underlying environment.

The majority of cell types used in the aforementioned studies (including fibroblasts, mesenchymal cells, epithelial cells, and peripheral nervous system cells) experience variable mechanical stimuli in vivo. Neural cells in the brain, in contrast, do not typically bear loads, and are mechanically isolated from the external environment by the cranium. Furthermore, native brain tissue is soft (elastic moduli, $E' \approx 500$ Pa) (16,17) compared with muscle ($E' \approx 10^4$ Pa) (13,18), connective tissue ($E' \approx 10^4$ Pa) (18), skin ($E' \approx 10^4$–10^5 Pa) (18,19), and bone ($E' \approx 10^9$–10^{10} Pa) (18,19). It is therefore unclear whether the mechanosensitive behavior observed in cells derived from stiffer tissues that are exposed to variable mechanical loads will be present in neural stem cells from the adult brain.

Recent work showed that primary neural cells from the brain, such as postnatal day 0 (PO) mouse hippocampal neurons (20) and mixed embryonic stage 17–19 (E1–E19) rat embryonic cortical progenitors (21), exhibit variable neuronal morphological differentiation and glial survival, respectively, on substrates of variable stiffness. Although these important studies shed light on neurogenesis in the embryonic and early postnatal brain, the extent to which substrate stiffness influences the fate decisions of a homogeneous neural stem cell population has not been explored. We analyzed the effects of substrate stiffness on the behavior of adult neural stem cells, a recently discovered cell population from the adult brain (22,23). Adult neural stem cells (aNSCs) have the capacity to differentiate into the three major cell types of the adult nervous system (24), are involved in new memory formation (22,25), respond to neural injury (22), and represent an important potential resource for a wide range of biomedical and neuroregenerative applications (26,27). In addition, aNSCs may encounter different mechanical environments in the adult brain (including gray and white matter, blood vessels, layered cell structures, and glial scars) which may present variable moduli ($E' \approx 10^2$–10^3 Pa) (17,28). Glial scarring in particular occurs after acute insults to the central

Submitted February 23, 2008, and accepted for publication July 17, 2008.

Albert J. Keung and Elizabeth F. Irwin contributed equally to this work.

Address reprint requests to Kevin E. Healy, Dept. of Materials Science and Engineering and Dept. of Bioengineering, 370 Hearst Memorial Mining Bldg., #1760, University of California at Berkeley, Berkeley, CA 94720-1760. Tel.: 510-643-3559; Fax: 510-643-5792; E-mail: kehealy@berkeley.edu; or to David V. Schaffer, Dept. of Chemical Engineering, 274 Stanley Hall, University of California at Berkeley, Berkeley, CA 94720-3220. Tel.: 510-643-5963; Fax: 510-642-4778; E-mail: schaffer@berkeley.edu.

Editor: Jason M. Haugh.

0006-3495/08/11/4426/13 $2.00

doi: 10.1529/biophysj.108.132217

nervous system (e.g., stroke, hemorrhage, traumatic injury, and infection), and is a process that requires attention and potentially management in regenerative medicine applications of the adult brain. Furthermore, the range of stiffness over which primary neuronal cultures were studied (20,21) was not previously extended below physiological stiffness (<250 Pa), and the extracellular matrix proteins used (generally laminin or fibronectin) present a number of receptor binding motifs that bind numerous adhesion receptors. Therefore, we studied the behavior and cell fate commitment of aNSCs in terms of mechanical signals on a biochemically well-defined substrate.

Our work builds upon a synthetic materials platform, termed an interpenetrating polymer network (IPN) (29–32). The IPN synthesis was modified such that substrate mechanical properties could be quantitatively modulated over a wide range, including stiffness above and below the regime relevant to neural tissue ($E' \approx 10^2$–10^3 Pa) (16,17). The proliferation or self-renewal, and multipotent differentiation, of aNSCs were analyzed in these variable moduli IPNs (vmIPNs). Results implicated a critical range of mechanical properties that modulate and support cell self-renewal, and bias cells toward neuronal versus glial differentiation. Intriguingly, optimal aNSC neuronal differentiation was observed near the mechanical properties of native brain tissue.

MATERIALS AND METHODS

Materials for vmIPN synthesis

Acrylamide (AAm), poly(ethylene glycol) 1000 monomethyl ether monomethacrylate (pEGMA), acrylic acid (AAc), acetic acid, *N*,*N*′-methylenebis (acrylamide) (BIS; ultrapure grade), and *N*,*N*,*N*′,*N*′-tetramethylethylenediamine (TEMED) were purchased from Polysciences, Inc. (Warrington, PA). We acquired *N*-hydroxysulfosuccinimide (sulfo-NHS), 2-(*N*-morpholino) ethanesulfonic acid, 0.9% sodium chloride buffer (MES; BupH MES Buffered Saline Pack), and sulfosuccinimidyl 4-(N-maleimidomethyl) cyclohexane-1-carboxylate (sulfo-SMCC) from Pierce (Rockford, IL). We obtained QTX ([3-(3,4-dimethyl-9-oxo-9H-thioxanthen-2-yloxy)-2-hydroxypropyl] trimethylammonium chloride), ammonium persulfate, and dichlorodimethylsilane from Sigma-Aldrich (St. Louis, MO). Methacryloxypropyltrimethoxysilane (MTMS) and allyltrichlorosilane (ATC) were obtained from Gelest (Morrisville, PA). Diamino-poly(ethylene glycol) ($PEG(NH_2)_2$; 3400 g/mol, chromatographically pure) was purchased from Nektar (Huntsville, AL). The arginine-glycine-aspartic acid (RGD) and arginine-glycine-glutamic acid (RGE) peptides were synthesized by American Peptide Co. (Sunnyvale, CA), and characterized using mass spectrometry and high-performance liquid chromatography (purities >95%). The RGD and RGE peptides were based on the integrin-binding sequence from rat-bone sialoprotein: acetyl-CGGNGEP-RGDTYRAY-NH_2 [**bsp-RGD(15)**] and acetyl-CGGNGEPRGETYRAY-NH_2 [**bsp-RGE(15)**] peptide, and acetyl-CGGNGEP**RGE**TYRAY-NH_2. All other chemicals were reagent-grade, and were used as purchased without further purification. All glassware was cleaned with a 2% solution of Contrad 70 (catalog number 04-355, Decon Laboratories, King of Prussia, PA) in water for 2 h, rinsed copiously with water, and baked dry. All water used in this study was ultrapure American Society for Testing and Materials (ASTM) type I reagent-grade water (18.2 MΩ-cm, pyrogen-free, endotoxin <0.03 EU/m) (33).

Cell culture surface preparation

Laminin cell culture surfaces were coated with poly-ornithine and saturated with mouse laminin I from the Engelbreth-Holm-Swarm sarcoma (Invitrogen, Carlsbad, CA), as described previously (34). For vmIPN synthesis, all reactions were carried out at room temperature unless otherwise stated. Glass coverslips (18-mm diameter, Fisher Scientific, Santa Clara, CA) were cleaned by submersion in ultrapure water (UPW) and sonicated for 30 min in UPW (Bransonic 5510, 40 kHz, 469 W, and 117 V, Branson Ultrasonic, Danbury, CT). This sonication step was repeated with acetone and again with UPW. After cleaning, samples were dried (N_2) and cleaned with an O_2 plasma (March Plasmod, Concord, CA) at 1 torr and 125 W for 5 min, to remove any adsorbed surface species. As described below, vmIPN was then grafted to the glass coverslip, using a two-step sequential photopolymerization developed from previously published protocols (29,30).

To activate glass substrates for synthesis, glass coverslips were treated with an organosilane to functionalize the surface for polymerization. Samples were covered in a 1% (v/v) methacryloxypropyltrimethoxysilane, 94% (v/v) methanol (MeOH), and 5% (v/v) water solution containing 5 μL of acetic acid. Samples were then rinsed 3 times in MeOH and baked for 30 min at 110°C. This activation method was compared with previously published glutaraldehyde activation methods (15).

For the first polymerization step of vmIPN synthesis, AAm gels were polymerized directly onto the functionalized glass coverslips. Solutions of 3–5% (w/v) AAm and varying amounts of BIS (0.3–0.03%, w/v) were produced in water. Polymerization was initiated by adding 10–20 μL of TEMED and 100 μL of 10% (w/v) ammonium persulfate (AP) per 10 mL of reactant solution. We pipetted 60 μL of this solution immediately onto the coverslips and covered it with glass ''coverdisks'' placed facedown on top of the monomer/cross-linker solution to create a smooth surface for cell culture. These glass coverdisks consisted of 18-mm-diameter coverslips, were treated with dichlorodimethylsilane for 1 min, and were wiped clean with Kimwipes (Sigma-Aldrich, St. Louis, MO) before use. Samples were allowed to polymerize for ~10–30 min. Then the coverdisks were removed, and samples were stored in water overnight.

An IPN was created by polymerizing a second layer of poly(ethylene glycol) (pEG) (~4 nm thick) within the top few nanometers of the first AAm layer. A solution of 0.02 g/mL poly(ethylene glycol)-1000-monomethylether (pEGMA), 0.0162 mL/mL AAc, and 0.01 g/mL BIS was initiated with 0.005 g/mL QTX in a degassed solution of 97:3 (v/v) water/isopropanol (IPA, Fisher Scientific) for 1 h, using an ultraviolet light transilluminator table (model TFL-40, Ultra-Violet Products, Upland, CA). The power of the table was measured at 2.3 mW/cm^2, using a radiometer (International Light, Peabody, MA) with a 352–377-nm bandpass filter. This resulted in an IPN with a high density of pEG at the surface (35).

Details regarding peptide grafting to the IPN can be found elsewhere (29,30), and are described briefly below. After formation of the IPN, samples were equilibrated with buffer (>30 min, MES, 0.5 M, pH 7). To functionalize the IPN with biological ligands, 3400 M_w $PEG(NH_2)_2$ spacer chains were grafted to the AAc sites via a carbodiimide reaction (1 h, 0.5 M MES, pH 7, 0.150 g/mL $PEG(NH_2)_2$, 0.005 g/mL EDC, 0.0025 g/mL Sulfo-NHS). After the reaction, the solution was aspirated, and samples were rinsed twice with 0.1 M MES buffer (pH 7.0), followed by two rinses with 50 mM sodium borate buffer (pH 7.5). At this point, the samples were sterilized by ultraviolet irradiation in a biosafety hood for 30 min. All subsequent solutions were sterile-filtered through a 0.22-μm filter. To couple bioactive molecules to the $PEG(NH_2)_2$-modified IPN, the heterobifunctional cross-linker, sulfo-SMCC, was reacted with the free amine on the $PEG(NH_2)_2$ chains (0.0005 g/mL sulfo-SMCC, pH 7.5, borate buffer, 30 min). The solution was then aspirated, and samples were rinsed twice with borate buffer, followed by two rinses with peptide-coupling buffer (sodium phosphate, 0.1 M, pH 6.6). Finally, the peptide (bsp-RGD(15) or bsp-RGE(15)) was coupled (20 μM) to the maleimide (sulfo-SMCC) at the peptide N-terminal free thiol. After the overnight reaction, the solution was aspirated, and samples were rinsed 4–5 times with coupling buffer, sonicated (UPW, 5 min), rinsed (UPW), and stored in phosphate-

buffered saline with 5000 U-μg/mL PennStrep (5000 U penicillin and 5000 μg streptomycin per milliliter) at 4°C.

Rheological materials characterization

During the AAm polymerization step of IPN synthesis, 5 mL of reactant solutions of AAm, BIS, TEMED, and AP were poured into a 60-mm-diameter polystyrene dish. The resulting bulk gels (~1 mm thick) were swollen in water overnight and then trimmed and loaded into a rheometer. Oscillatory shear measurements of polyacrylamide (pAAm) gels were performed on a rheometer (MCR300, Anton Paar, Ashland, VA) with 50-mm parallel plates at a gap height of 0.5–3.0 mm. A humidity chamber was placed around the sample to prevent dehydration. The lower plate temperature was regulated with a Peltier heating element connected to a recirculating water bath. Frequency sweeps from 0.001–10 Hz at 5% strain were performed first at 25°C, and then at 37°C. No significant difference in complex modulus was seen between the two temperatures. The elastic modulus, E', was estimated as $E' = 2G'(1 + \nu)$, where G' is the complex storage modulus at 1 Hz as measured by the rheometer and ν is Poisson's ratio, assumed to be 0.5. Results from atomic-force measurements on vmIPNs and rheological measurements on the bulk polyacrylamide gels showed good agreement (35). Furthermore, the modulus of the polyacrylamide layer and the full vmIPN were not statistically different (35). In addition, we assumed that the E' for tissue-culture polystyrene was $\sim 10^9$ Pa, as measured previously (36).

Neural stem-cell culture

Neural stem cells were isolated from the hippocampi of adult female Fischer 344 rats as previously described (24), and were used between 10–30 passages of culturing. Cells were seeded (1500 cells/cm^2 for proliferation; 25,000 cells/cm^2 for differentiation) onto peptide-modified vmIPNs or laminin-modified culture wells, and incubated (37°C, 5% CO_2) in serum-free media consisting of Dulbecco's modified Eagle medium (F-12/DMEM, high glucose, with L-glutamine, with pyridoxine hydrochloride, and without sodium pyruvate; Invitrogen) with N-2 supplement (Invitrogen). These media were supplemented with various soluble factors to modulate cell behavior: 20 ng/mL FGF-2 (Invitrogen) for cell proliferation, 1 μM retinoic acid (BioMol, Plymouth Meeting, PA) with 5 μM forskolin (BioMol) for neuronal differentiation, or 1 μM retinoic acid with 1 v/v % fetal bovine serum (Invitrogen) for mixed glial and neuronal differentiation. Wells were rinsed every 48 h with fresh media. The self-renewal and differentiation of these exact cells on IPNs grafted to polystyrene were described previously (29) and compared with laminin-coated polystyrene.

Immunofluorescence assays

For immunofluorescence staining, cells were cultured for 5–6 days and fixed with 4% paraformaldehyde (Fisher Scientific), blocked for 1 h with 2% goat serum (Sigma-Aldrich), permeabilized with 0.3% Triton X-100 (Calbiochem, San Diego, CA), and incubated for 36 h with primary antibodies rabbit anti-nestin (1:500 dilution; AbCam, Cambridge, MA), mouse anti-β-tubulin III (1:500 dilution; Sigma-Aldrich), and guinea pig anti-glial fibrillary acidic protein (GFAP; 1:1000 dilution; Advanced Immunochemical, Long Beach, CA). The primary antibody solution was then removed, and cells were rinsed and incubated for 1.5 h with Alexa Fluor secondary antibodies: 488 goat anti-rabbit immunoglobulin G, 546 goat anti-mouse immunoglobulin G, and 647 goat anti-guinea pig immunoglobulin G at a dilution of 1:500 (all from Invitrogen). Nuclei were stained with DAPI (Invitrogen). Images were collected on a Nikon Eclipse TE2000-E and a Zeiss META 510 laser scanning confocal microscope.

Quantitative real-time polymerase chain reaction assay

Quantitative real-time polymerase chain reaction (QRT-PCR) was used as a complementary technique to immunofluorescent staining, for accurate quantification of specific mRNA concentrations in cells grown on vmIPNs and laminin (using an iCycler 4, Bio-Rad Laboratories, Hercules, CA) (37). Cells were lysed and frozen in TRIZOL (Invitrogen), and mRNA was extracted and reverse-transcribed to cDNA using the ThermoScript RT-PCR System for First-Strand cDNA Synthesis (Invitrogen). The QRT-PCR assay used GFAP as a marker for astrocytic differentiation of progenitor cells, β-tubulin III as a marker for neurons, and nestin as a marker for aNSCs. Equivalent amounts of total RNA were transcribed into cDNA, which were subsequently used as templates for each QRT-PCR reaction. To normalize any remaining variations in starting cDNA amounts, each reaction was carried out in duplex format, with ribosomal 18S detected using Cal-Dye TaqMan probes (Biosearch Technologies, Novato, CA). The lineage marker was detected using FAM-Dye TaqMan probes (Biosearch Technologies). Duplicate QRT-PCR reactions were run for each biological sample, where $n = 5$–6 for each condition.

The primers and TaqMan probes included: GFAP, 5′-GACCTGCGACCTTGAGTCCT-3′, 5′-TCTCCTCCTTGAGGCTTTGG-3′, 5′-FAM490-TCCTTGGAGAGGCAAATGCGC-BHQ-3′; β-tubulin III, 5′-GCATGGATGAGATGGAGTTCACC-3′, 5′-CGACTCCTCGTCGTCATCTTCATAC-3′, 5′-FAM490-TGAACGACCTGGTGTCTGAG-BHQ-3′; nestin, 5′-GAGCTCTCTGGGCAAGTGGA-3′, 5′-CTCCCACCGCTGTTGATTTC-3′, 5′-FAM490-AGGACAGTCAGCAGTGCCTGCA-BHQ-3′; and 18S, 5′-GTAACCCGTTGAACCCCATTC-3′, 5′-CCATCCAATCGGTAGTAGCGA-3′, 5′-CAL610-AAGTGCGGGTCATAAGCTTGCG-BHQ-3′. Standards for performing QRT-PCR were pPCR4-TOPO plasmids (Invitrogen), containing the amplicon of interest as an insert. The plasmids were linearized by restriction digest and quantified by absorbance, and 10-fold serial dilutions from 1 ng/μL to 10^{-9} ng/μL were prepared to generate a standard curve.

Image analysis

To assay self-renewal, aNSCs were seeded at 1500 cells/cm^2 on various surfaces and grown for 3–6 days, and phase-contrast images were taken every 12–24 h of culture. Cell number was determined by image analysis of phase contrast and bright-field images of cells. Image analysis used ImageJ or CellProfiler software (38). The image-analysis method was validated by using the CyQUANT assay (Invitrogen), following the manufacturer's instructions (data not shown).

Each cell in the differentiation immunostaining experiments was scored manually as positive for neuronal or glial markers with $n = 3$ biological replicate wells per condition. In the neuronal differentiation experiment, β-tubulin III intensity histograms were generated in CellProfiler software (38). Primary objects/cells were identified by DAPI staining, and the average intensity of pixels within a circle with a set radius around the primary object was measured. Three biological replicate wells ($n = 3$) were used per condition. Samples without primary antibody added but with only secondary antibody were used as negative controls to measure background fluorescence. All images, including negative controls, were processed, and the negative-control levels were then subtracted from all images. The β-tubulin III staining of cells cultured in 1 μM retinoic acid and 5 μM forskolin on laminin-coated polystyrene was used to produce positive controls (24). Cells on gels with similar intensities were scored β-tubulin III-positive. Likewise, GFAP staining of cells cultured in 1 v/v % fetal bovine serum (FBS) on laminin/polystyrene was used to produce positive controls (24). Relative numbers of marker-positive cells are shown in Fig. 5.

RESULTS

Synthesis of vmIPNs

A primary objective and central need of this work was to create materials with variable moduli *and* defined and adjustable surface chemistry (Fig. 1 *A*). We modified the synthesis of well-studied IPNs to control the modulus within a range of 10–10,000 Pa, while allowing peptide modification

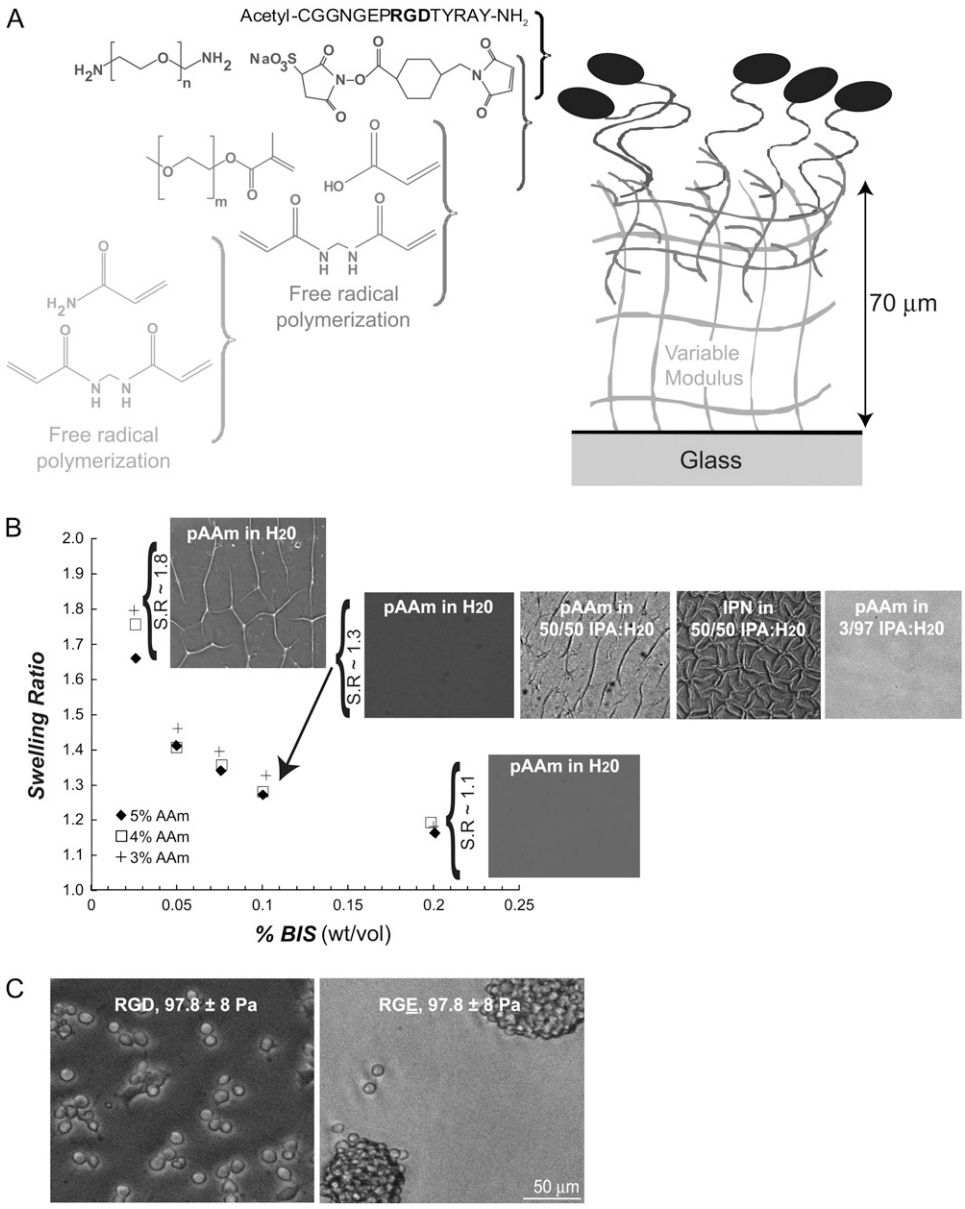

FIGURE 1 Synthesis of a vmIPN and characterization. (*A*) Schematic of sequential polymerizations and grafting chemistry used to synthesize the vmIPN. Drawing not to scale. Molecular weights of the CH_2CH_2O repeat for *m* and *n* are 1000 and 3400, respectively. (*B*) Swelling behavior of first poly(acrylamide) (pAAm) layer in water. Swelling ratio (S.R.) is calculated as in Table 1. After swelling in water, surface features appeared in the first vmIPN pAAm layer of low moduli (e.g., <1000 Pa for 10 wt% gels) which have high swelling ratios. The pAAm layers shown at S.R.~1.8 were 13.5 ± 1 Pa. After 10 min in a 50/50 v/v water:isopropyl alcohol (IPA) solution, surface morphology was altered in the first vmIPN pAAm layer of low moduli (e.g, <1000 Pa for 10 weight % gels) which have high swelling ratios. After the second polymerization of the vmIPN, surface features persisted in 50:50 v/v isopropyl alcohol (IPA)/water solvent conditions, but were absent in 3:97 v/v IPA/water solvent conditions. (*C*) The aNSC response was specific to peptide ligand on vmIPNs. The aNSCs adhere and proliferate on bsp-RGD(15) peptide-modified vmIPNs, whereas they form nonadherent cell aggregates on bsp-RGE(15) peptide-modified vmIPNs. Both substrates have an elastic modulus of 97.8 ± 8 Pa (Table 1). These phase-contrast images were taken after 3 days of culture in FGF-2 proliferating media conditions.

of the interface to modulate cell adhesion. Table 1 lists the conditions used for the first polymerization in the synthesis scheme that defined the mechanical properties of our vmIPNs. Free-radical polymerization occurred in the reactant solution well above the underlying glass support, and created a network ~70 μm thick (characterized by Irwin et al. (35)).

The poly(acrylamide) (pAAm) networks created in situ via free-radical polymerization exhibited a high degree of swelling when immersed in aqueous solvents. Both swelling and rheological measurements were made on bulk pAAm gels of ~60-mm diameter and 1-mm thickness, which were polymerized in parallel during vmIPN AAm layer polymerization (Fig. 1 and Table 1). The swelling of pAAm gels in water increased as the weight % of BIS cross-linker decreased in the reactant mixture (Fig. 1 *B*). When pAAm network formulations that exhibited a high swelling ratio were formed on top of both methacryl and glutaraldehyde activated glass, surface defects appeared after immersing in aqueous media overnight (Fig. 1 *B*). No difference in both the presence and spatial pattern of surface defects was seen between the methacryl-mediated and glutaraldehyde-mediated surface chemistries (data not shown). To overcome this problem, formulations in Table 1 were optimized to have a low swelling ratio (i.e., a high weight % BIS), while modulating the weight % AAm to tune the moduli to a desired value. Note that in the ~10-Pa formulation, the swelling ratio is high, because all other reactant formulations attempted for this extremely soft gel failed to polymerize reliably in ambient conditions. Because of the high swelling ratio, surface defects were seen on some portions of the ~10-Pa vmIPN formulation listed in Table 1. However, all subsequent conclusions about cell behavior could be drawn by observation

TABLE 1 Tuning the vmIPN moduli to those of neural tissue

Weight % AAm	Weight % BIS	Swelling ratio	Measured elastic modulus (Pa) of swollen pAAm network (± SD) ($n = 3$)
10.0	0.300	1.11	9580 ± 767
10.0	0.150	1.18	5460 ± 290
5.00	0.200	1.10	902 ± 71
4.00	0.200	1.15	431 ± 26
3.00	0.100	1.25	97.8 ± 8
3.00	0.025	1.80	13.5 ± 1

By manipulating the concentration of monomers acrylamide (AAm) and bisacrylamide (BIS), poly(acrylamide) (pAAm) gels were synthesized to range in modulus from ~10 to 10,000 Pa. These formulations were chosen to minimize the swelling ratio of these gels (Fig. 1 *B*). Polymerizations were conducted in 10-mL batches. The 10 weight % AAm formulations utilized 20 μL TEMED and 100 μL of 10 weight % AP, whereas all other formulations used 6 μL TEMED and 50 μL AP. Swelling ratio was calculated as the ratio of the diameter of the AAm network after >12 h of swelling in ultrapure water versus the diameter of the initial in situ polymerized diameter. Elastic modulus was determined through rheology (see Materials and Methods).

of aNSC behavior on areas of ~10-Pa vmIPN samples that were flat without surface defects, and any exceptions are specifically noted.

After optimizing the first polymerization in the vmIPN synthesis scheme (Table 1), a second poly(ethylene-glycol) and acrylic-acid polymerization was conducted in a novel solvent system. For soft (<1000 Pa) pAAm networks on glass, simple immersion of the pAAm network in a 50:50 v/v % isopropyl alcohol/water solution, the solvent previously used for the second polymerization (29,30), induced formation of surface defects (Fig. 1 *B*). Subsequent polymerization of the second, interpenetrating p(EG-co-AAc) layer under these poor solvent conditions effectively ''locked'' these surface features in the pAAm network into place (Fig. 1 *B*). We reduced the 50:50 v/v % isopropyl alcohol/water solvent from previous protocols to a 3:97 v/v % ratio, which eliminated these surface features (Fig. 1 *B*). Subsequent peptide-grafting to the vmIPN followed previously published protocols (29,30). Surface chemical composition, as monitored by C 1-s, N 1-s, O 1-s, and Si 1-s peaks by x-ray photoelectron spectroscopy and fluorescent peptide surface density, did not vary with modulus in surfaces prepared using these methods (35). These vmIPNs defined a thick, flat substrate with a tunable, well-characterized chemistry for our subsequent studies with aNSCs.

aNSC self-renewal on vmIPNs

The aNSCs isolated from adult rat hippocampi (34) were first cultured on vmIPNs under media conditions that promoted proliferation (24) (Figs. 1 *C* and 2). Importantly, aNSCs responded specifically to the grafted ligand for all formulations in Table 1, because no aNSCs attached to RGE-modified vmIPNs, and they instead formed nonadherent spheres (data not shown; Fig. 1 *C*). In other words, aNSCs attached effectively to all RGD-modified vmIPNs (data not shown), and spread well on vmIPNs of moduli greater than ~100 Pa soon after seeding (data not shown). In addition, no difference in cell morphology was seen during proliferation on vmIPNs of ≥100 Pa versus laminin coated polystyrene (data not shown; Fig. 2 *A*). By contrast, on ~10-Pa vmIPNs, aNSCs did not disperse well, and grew in adherent clusters during the entire course of the experiment (data not shown; Fig. 2 *A*).

Lineage markers were analyzed by immunofluorescence to assess cell-differentiation state. After 5 days of culture in proliferating media conditions, cells were fixed and stained to analyze protein markers for three lineages: immature stem cells, mature astrocytes, and mature neurons. All cells expressed high levels of the progenitor cell marker protein nestin, and low levels of the astrocytic and neuronal marker proteins, GFAP and β-tubulin III, respectively (Fig. 2 *B*). Therefore, under proliferating media conditions, all vmIPN substrates maintained the immature cell properties of the harvested nestin$^+$ aNSC population.

To quantify cell-proliferation rate, cell number was determined by analysis of phase-contrast images taken every 12–24 h during culture for 5 days, and was fit to a Verhulst logistic growth model (Fig. 2 *C*). The Verhulst model assumes exponential growth with contact inhibition, and contains only three parameters: effective growth rate, maximal substrate carrying capacity, and initial cell number. Both the carrying capacity and initial cell number were determined experimentally, by counting cells in an aNSC confluent layer and counting cells 2 h after seeding for each sample, respectively. The vmIPNs of moduli ≥100 Pa supported robust proliferation, as indicated by only modest changes of effective growth rate, r, with time in this range (Fig. 2 *C*). However, aNSCs divided much more slowly, and in clusters, on ~10-Pa IPNs (Fig. 2). Interestingly, a slight peak in cell proliferation was observed between 1–4 kPa, near the stiffness of native brain tissue (17,28).

aNSC differentiation on vmIPNs

In addition to self-renewal, aNSCs can exhibit multipotent differentiation into glial and neuronal lineages in vivo (39) and in vitro on laminin coated polystyrene dishes (24). To determine the ability of vmIPNs to support multipotent differentiation, we seeded aNSCs in media containing 1 v/v % FBS, a condition shown to drive astrocytic differentiation on hard surfaces (24,40). Control conditions included aNSCs on laminin-coated polystyrene either in 1 v/v % FBS or in the presence of 1 μM retinoic acid and 5 μM forskolin, which strongly promote neuronal differentiation. The aNSCs attached to and spread well on all RGD-modified vmIPNs of moduli greater than or equal to ~100 Pa soon after seeding (Figs. 3 *A* and 4 *A* and *C*), though aNSCs on ~10-Pa IPNs did not spread as well, and clustered during differentiation (Fig. 3, *B* and *C*).

Quantitatively, equal numbers of aNSCs attached initially to all surfaces (Figs. 3 *A* and 4 *A–C*). Cell number then reached a brief plateau at day 1, likely representing cell-cycle

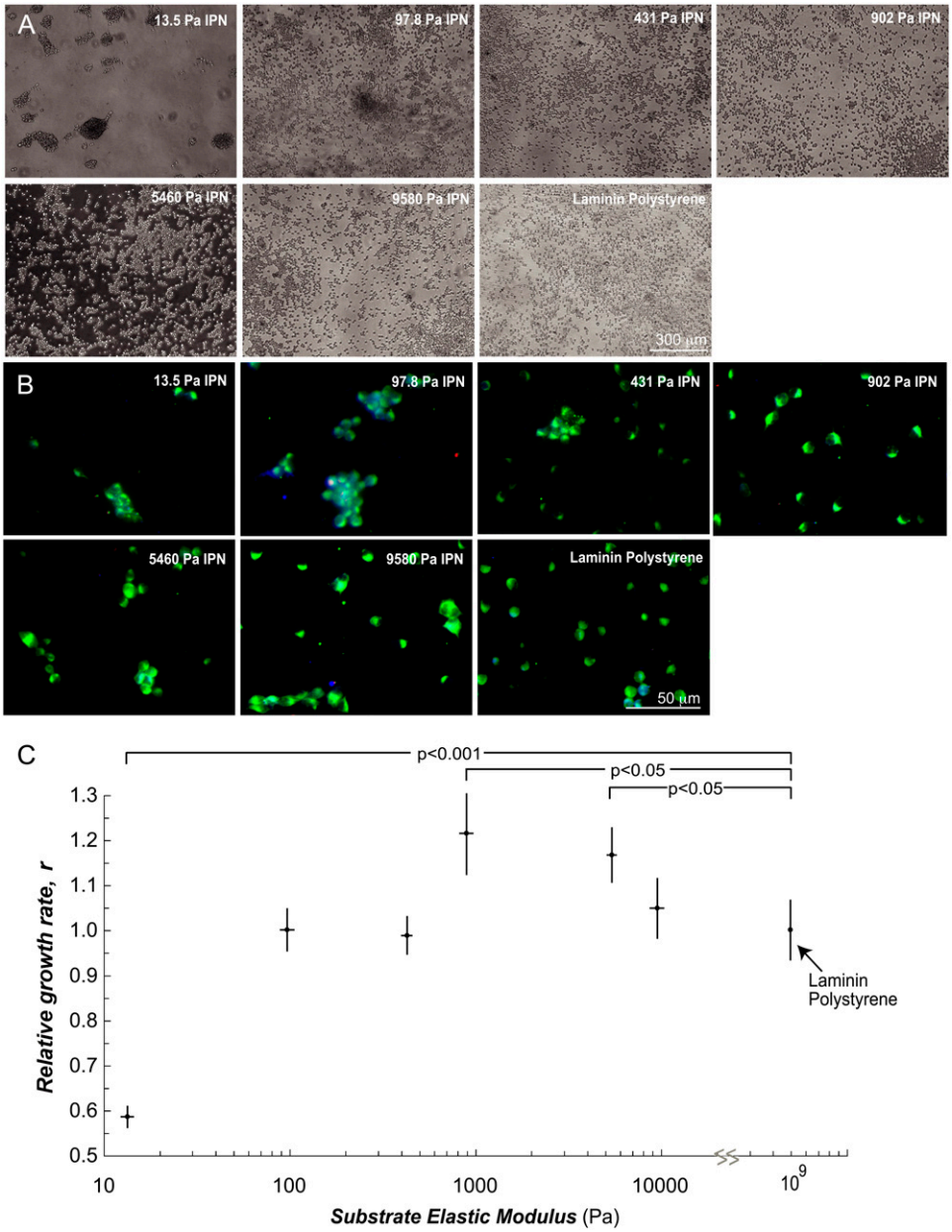

FIGURE 2 The aNSCs self-renew on vmIPNs of ≥100 Pa. (*A*) Phase-contrast images of aNSCs on vmIPNs in media conditions that promoted self-renewal (20 ng/mL FGF-2). (*B*) Immunocytochemistry confirmed that all cells contained the progenitor cell marker, nestin (*green*), and low levels of β-tubulin III (*red*) and GFAP (*blue*), which appear as faintly purple cells. (*C*) Growth rate of undifferentiated stem cells as a function of substrate elastic modulus. The aNSC number with time on vmIPNs was fit to a Verhulst logistic growth model ($n = 3$). Growth rates are normalized to laminin polystyrene substrates ($r = 0.33$–0.39 1/h; doubling time, $1/r = 25$–30 h; carrying capacity, 6.6×10^5 cells/cm^2 or 3800 cells per image). Error bars are 95% confidence intervals, and p-values <0.05, based on Student's t-test under laminin-coated polystyrene surface conditions, are shown.

arrest, and modestly decreased through day 6. This gradual reduction in cell number on laminin-polystyrene surfaces with serum or forskolin/retinoic acid likely indicates that a fraction of cells was unable to undergo full differentiation into astrocytes or neurons, respectively, indicating a modest cell selection during the differentiation process. On the vmIPN surfaces, final cell number gradually decreased with decreasing stiffness, indicating that cells did not survive or proliferate as effectively on softer surfaces under conditions that promote astrocytic differentiation (Fig. 4 *C*).

The extent of glial differentiation at 6 days was quantitatively analyzed on different moduli (Fig. 4 *B*), and GFAP staining intensity was divided into high and low bins (Fig. 4 *D*). This analysis indicates that the extent of maturation of astrocytic (GFAP+) cells is constant over moduli, because no statistically significant differences in GFAP staining were observed with modulus (Figs. 3 *C* and 4 *D*).

We also analyzed cell differentiation as a function of modulus under strong proneuronal media conditions (1 μM retinoic acid and 5 μM forskolin), shown to bias differentiation heavily toward neurons on laminin and stiff IPN substrates (29,40). The aNSCs again attached effectively to all RGD-modified vmIPNs in this neuronal differentiation media (data not shown), and spread well on IPNs of moduli greater than ~100 Pa soon after seeding (data not shown). However, on ~10-Pa IPNs, NSCs differentiated in clusters (Fig. 5 *A*). We analyzed the quality of neuronal differentiation after 6 days by measuring both β-tubulin III protein and gene expression levels via quantitative immunofluorescence analysis and QRT-PCR, respectively (Fig. 5, *B* and *C*). Be-

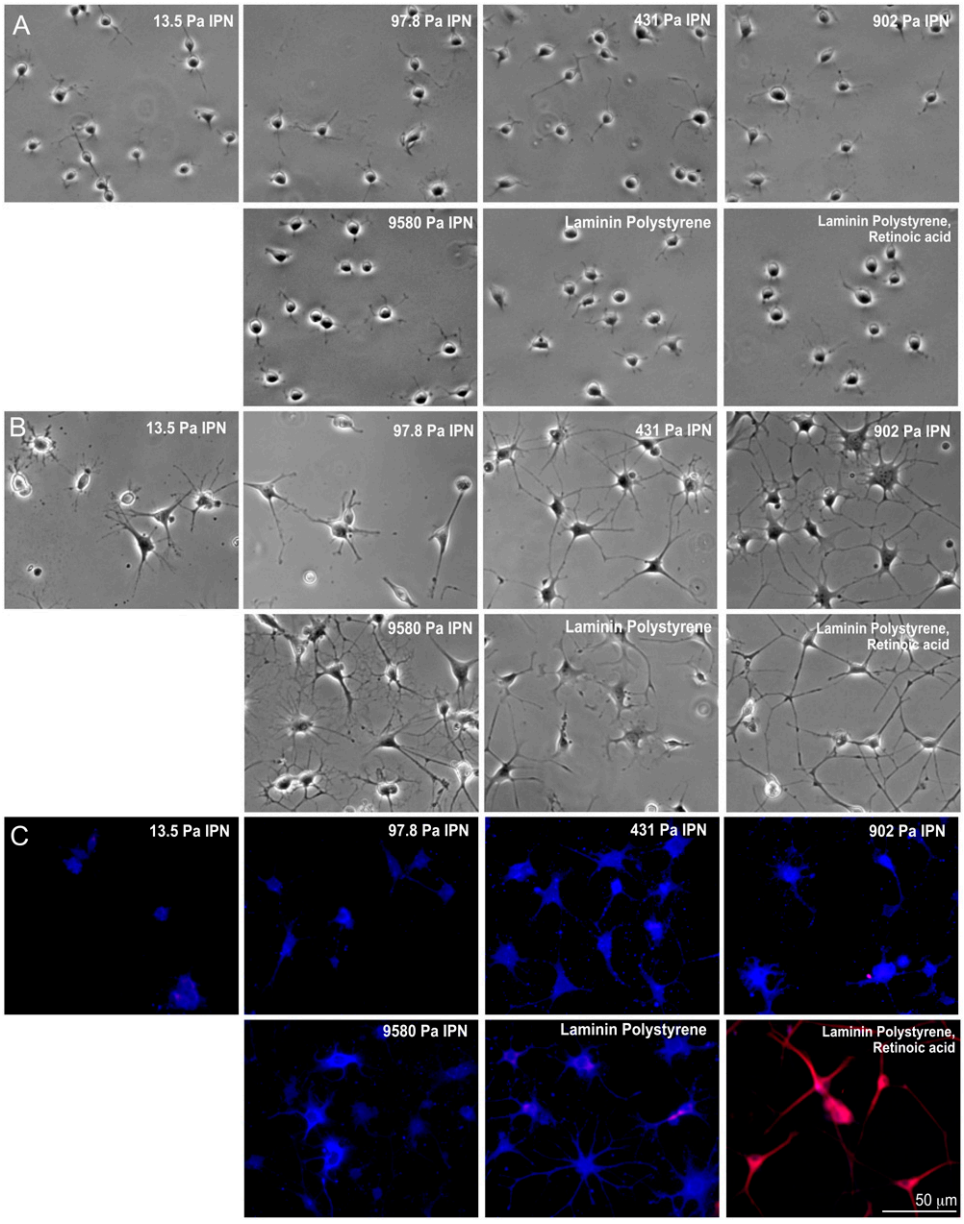

FIGURE 3 The aNSCs differentiate on vmIPNs into glia over a wide range of moduli. (*A*) Phase-contrast images of aNSCs 4 h after seeding onto various substrates in glial media conditions (1 v/v % fetal bovine serum). Shown also are control conditions with neuronal media on laminin-coated polystyrene substrates (1 μM retinoic acid and 5 μM forskolin; no serum). (*B*) Phase-contrast images of aNSCs after 6 days of differentiation in glial media conditions. (*C*) Immunostaining of aNSCs after 6 days of differentiation in glial media conditions. Cell lineage markers: progenitor cell marker nestin (*green*), mature neuronal marker β-tubulin III (*red*), and astrocytic marker GFAP (*blue*).

cause the cultures were composed solely of neurons, both of these methods provided information on the average β-tubulin III expression per cell. Quantitative real-time PCR revealed an optimum in neuronal differentiation on ~500-Pa vmIPNs, as indicated by the peak in β-tubulin III expression in Fig. 5 *C* (*left axis*), whereas expression of GFAP, an astrocytic marker, remained low across all moduli (data not shown). Immunofluorescence staining to analyze marker expression at the single-cell level indicated that nearly all cells were positive for β-tubulin III across all substrates, but cells from each sample exhibited a range of β-tubulin III intensities. Intensity histograms for each image were analyzed, and the number of cells with high β-tubulin III staining intensity (Fig. 5 *C*, *right axis*) correlated well with QRT-PCR expression results. These results show that below physiological stiffness, neuronal mRNA and protein expression decreases.

Finally, we analyzed whether, under conditions where cells ordinarily differentiate into a mixture of neurons and astrocytes (1 μM retinoic acid + 1 v/v % serum), substrate stiffness could bias the lineage of the differentiated cell population. When retinoic acid was added to serum-containing media, the softest substrates showed a greater percentage of cells positive for the neuronal marker β-tubulin III, and a lower percentage of glial GFAP-positive cells (Fig. 6 *B*). Strikingly, as the substrates became stiffer, more glia and fewer neurons were observed. Both the increase in glia and decrease in neurons with stiffer substrates appeared to be monotonic, with approximately equal numbers of glia and neurons produced from

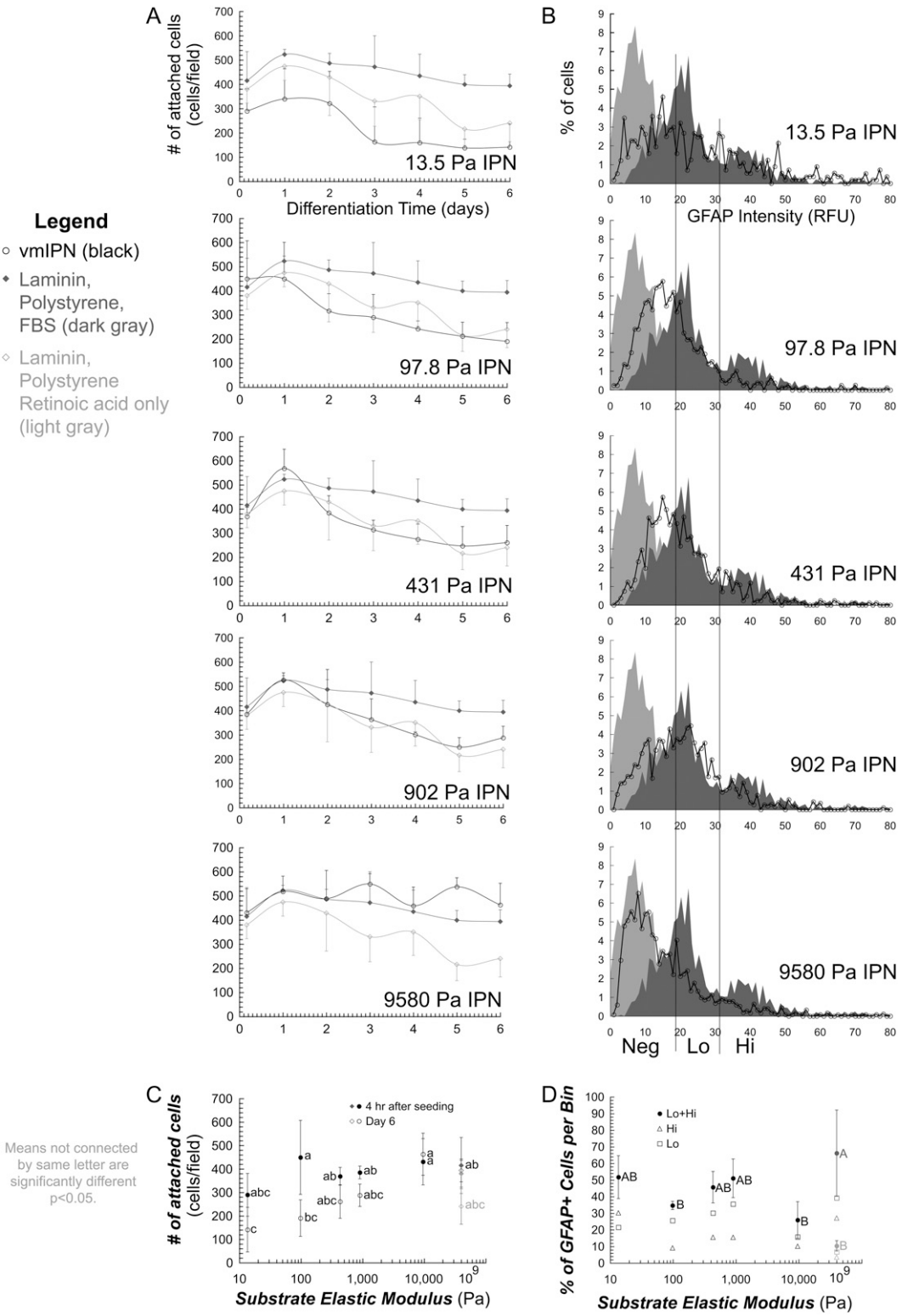

FIGURE 4 Survival and maturity of glial cell types are modestly affected by substrate modulus. (*A*) Number of attached cells on various substrates, differentiated under glial media conditions (1 v/v % fetal bovine serum), black in all plots. In all plots, dark gray is laminin-coated polystyrene. Shown also are control conditions with neuronal media on laminin-coated polystyrene substrates (1 μM retinoic acid + 5 μM forskolin; no serum), which are light gray in all plots. (*B*) Histograms indicate number of cells at particular GFAP staining intensities. All images were taken after 6 days of culture. (*C*) Summary of *A*. Number of attached cells as a function of modulus at 4 h after seeding, and after 6 days of differentiation. (*D*) Summary of *B*. Percentage of cells that stained positive for GFAP for each intensity bin. For *A*, *C*, and *D*, error bars are 95% confidence intervals. Means with same group letter are not significantly different from each other (analysis of variation Tukey-Kramer test, $p < 0.05$). Note the log *x*-axis in *C* and *D*.

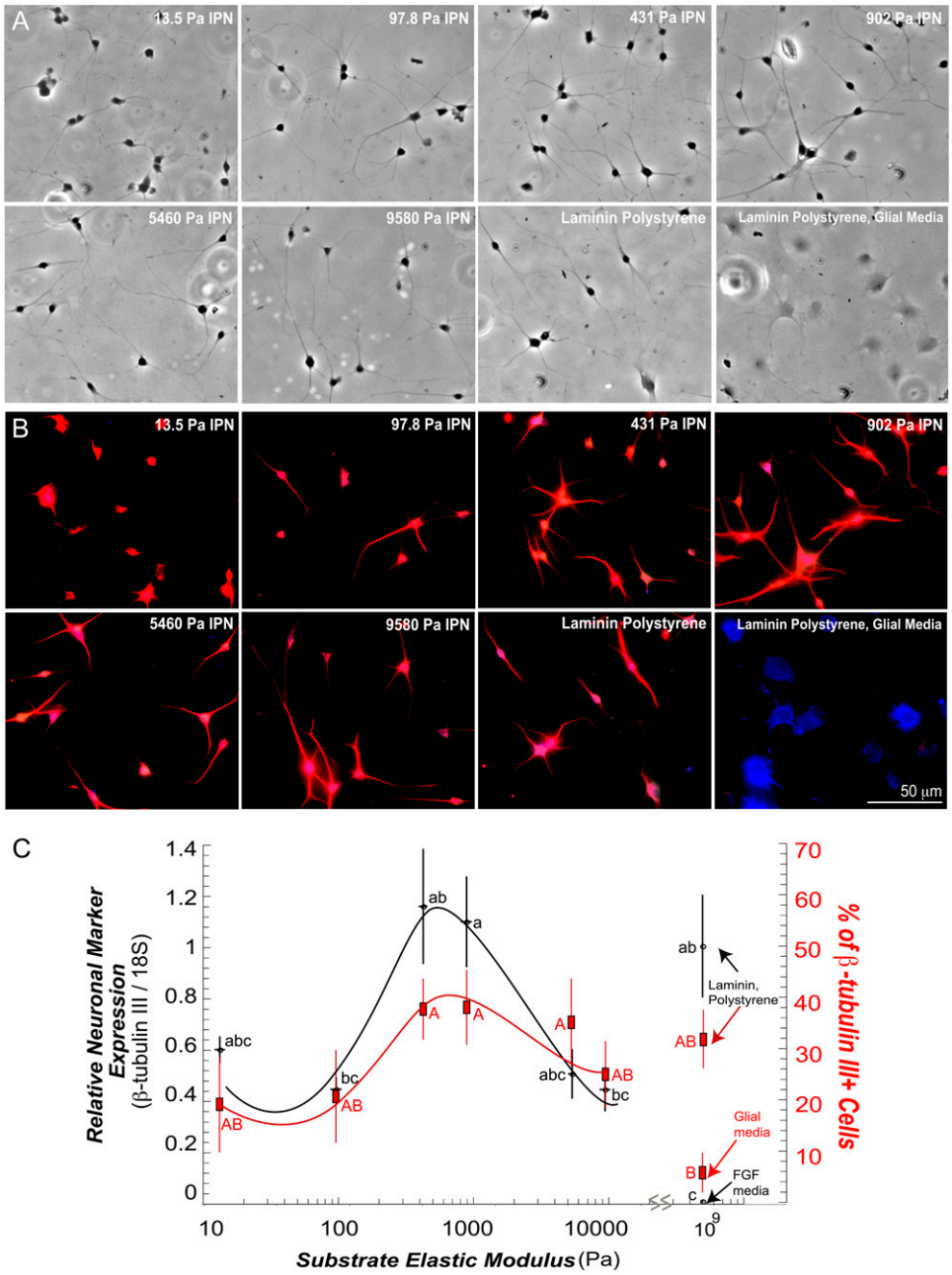

FIGURE 5 The aNSCs differentiate on vmIPNs into neurons at ~500 Pa. (*A*) Phase-contrast images of aNSCs differentiated under neuronal differentiation conditions (1 μM retinoic acid and 5 μM forskolin). On ~10-Pa vmIPNs only, defect sites are created because of high swelling (see Results). Cells on such sites are excluded from image analysis in *C*. (*B*) Immunostaining of aNSCs differentiated under neuronal differentiation conditions. Cell lineage markers: progenitor cell marker nestin (*green*), mature neuronal marker β-tubulin III (*red*), and astrocytic marker GFAP (*blue*). (*C*) On left axis, β-tubulin III expression as a function of substrate modulus was assayed by QRT-PCR ($n = 5$–6). Note the log *x*-axis and peak in β-tubulin III near 500 Pa. On right axis (*red*), the percentage of cells that fell above a threshold of β-tubulin III intensity (*red* in *b*) is shown. Error bars are 95% confidence intervals. Means with same group letter are not significantly different from each other (analysis of variation Tukey-Kramer test, $p < 0.05$). The QRT-PCR value for the ~10-Pa vmIPN includes cells on surface defects, and therefore likely overestimates β-tubulin III expression. All images were taken after 6 days of culture. Glial media label indicates DMEM/N-2 media supplemented with only 1 v/v % FBS on laminin-coated polystyrene.

aNSCs at ~1000 Pa. It should also be noted that all vmIPNs exhibited at least a 15% greater percentage of neurons than the control laminin-coated polystyrene surface (Fig. 6). These results indicate that vmIPNs ~100 Pa and stiffer can support both neuronal and glial differentiation, but interestingly, softer gels either instruct neuronal lineage commitment, or select for neuronal over glial cell survival.

DISCUSSION

We examined the self-renewal and differentiation of aNSCs in well-defined biochemical and mechanical microenvironments. By developing a synthetic cell culture platform, we were able to vary the range of mechanical properties of the substrate by three orders of magnitude, spanning a range of elastic moduli above and below that of native brain tissue. The aNSC self-renewal was well-supported on vmIPNs of ~100–10,000 Pa. Under conditions that induce neuronal differentiation, differentiation peaked on vmIPNs of ~500 Pa, the approximate modulus of the hippocampus (17). Cells differentiating into astrocytes did not survive well on softer surfaces, though the extent of astrocytic differentiation did not vary with modulus. Finally, under conditions that induced mixed differentiation, the fraction of glial cells

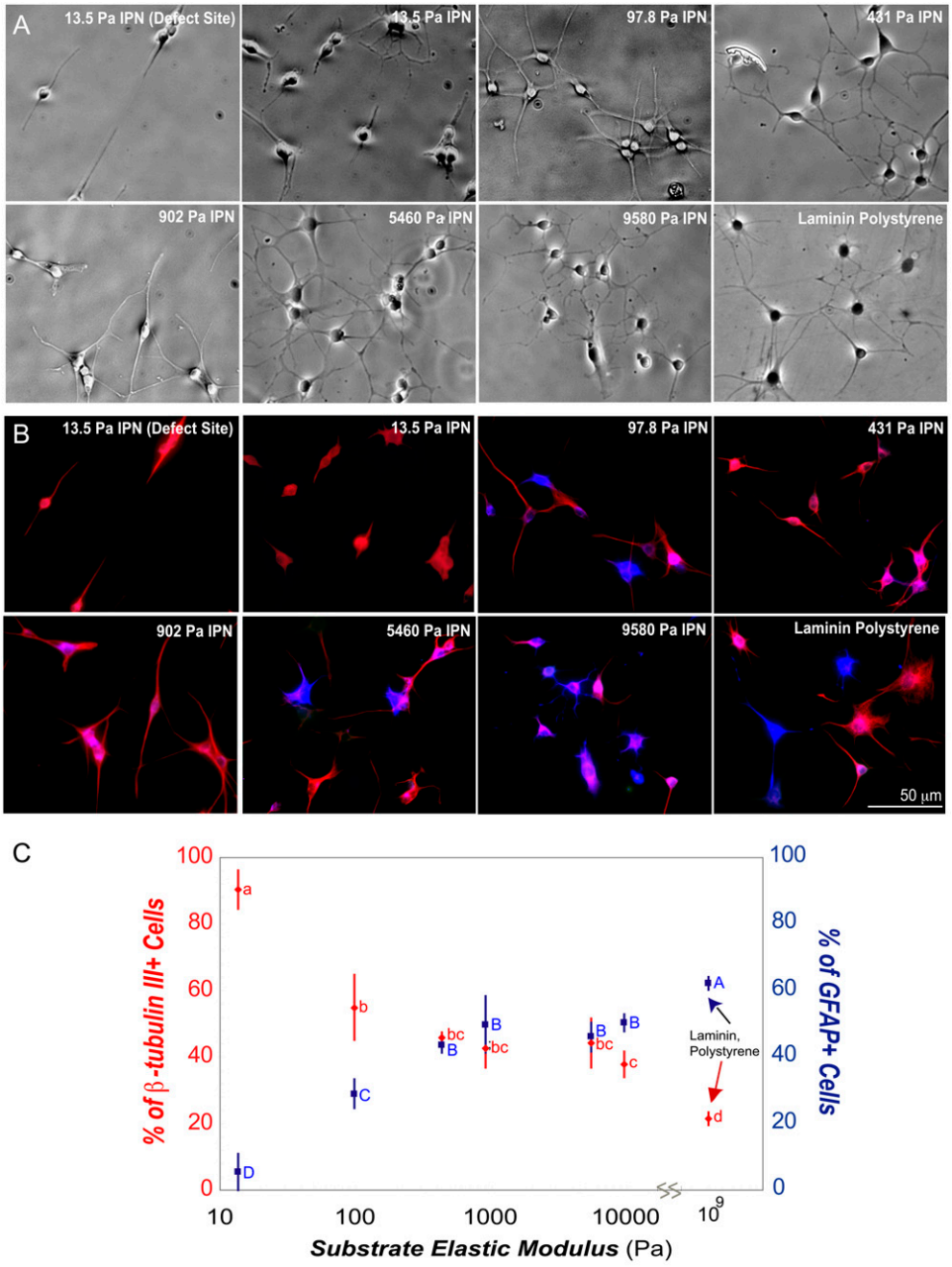

FIGURE 6 The proportion of neurons versus glia under mixed differentiation is a strong function of modulus. (*A*) Phase-contrast images of aNSCs differentiated under mixed glial and neuronal differentiation conditions (1 μM retinoic acid and 1 v/v % fetal bovine serum). (*B*) Immunostaining of aNSCs differentiated under mixed differentiation conditions. Cell-lineage markers: progenitor cell marker nestin (green), mature neuronal marker β-tubulin III (*red*), and astrocytic marker GFAP (*blue*). (*C*) Percentage of cells that stained positive for β-tubulin III (*red*) is on left axis, and for GFAP (*blue*), on right axis. Error bars are 95% confidence intervals. Means with same group letter are not significantly different from each other (analysis of variation Tukey-Kramer test, $p < 0.05$). Note the log *x*-axis. All images were taken after 6 days of culture.

monotonically decreased and neurons increased in mixed differentiation conditions as vmIPNs became progressively softer. Therefore, modulus and soluble factors can be combined to control the composition and extent of differentiation of neural stem-cell cultures.

In general, the vmIPN represents a versatile platform to tune independently both the biochemical and mechanical properties of a culture substrate (Fig. 1 *A*). Both soluble and substrate biochemical signals, which are important regulators of stem-cell behavior (29,41,42), can function via ligand-receptor engagement at the substrate-cell interface. However, it is preferable to employ well-defined signals to control this interface, because serum and animal-derived or human-derived ECM proteins, for example, can obfuscate efforts to study substrate-mediated signaling. Serum proteins can adsorb to surfaces in a manner that is difficult to control, and ECM proteins have variable isoforms, splice forms, and glycoforms of unknown signaling properties. Our vmIPN was engineered to avoid these issues and promote specific ligand-receptor engagement between the bsp-RGD(15) and the $\alpha_v\beta_3$ integrin (29). Furthermore, the substrate ligand motif can readily be varied in this system, enabling analysis of the capacities of different cell-surface receptors in mechanotransduction. In addition, previous protocols to create sub-

strates with variable moduli typically used AAm polymerization on an activated glass substrate (15,20,43). The resulting immobilized pAAm network can swell substantially to create surface defects (Fig. 1 *B*), particularly at low moduli. These features represent obstacles to using low-moduli pAAm substrates, e.g., aNSCs preferentially migrate into and are retained within the surface defects of culture substrates that are swollen in aqueous media conditions (data not shown). In this study, the monomer weight % was optimized to minimize swelling. Furthermore, IPN chemistry synthesis and sterilization conditions were modified from earlier protocols (29,30) to avoid changes in the surface morphology attributable to the swelling of polymer networks. The sequential chemistry of the vmIPN allows facile conjugation of many ligands over a large range of surface densities, a feature previously demonstrated with traditional IPNs (29,30). Moreover, vmIPNs offer the capacity to create ligand arrays, using techniques that were successful on glass substrates for embryonic cortical progenitors (41). The vmIPN platform was recently used with activated monocytes (35), and can readily be extended to other cell types.

The behavior of aNSCs differed markedly between extremely soft culture substrates ($E' \sim 10$ Pa) versus all other substrates of higher moduli (Figs. 2–6). The aNSCs attached to ~10-Pa substrates, but remained highly rounded and clustered (Fig. 2 *A*). Hippocampal glial cells and tissue have elastic moduli of ~100 and 300 Pa, respectively (17), well above the 10-Pa substrate, signifying that appropriate aNSC adhesion does not occur below the stiffness of the native microenvironment. These results also suggest that cytoskeletal compressive and tensile elements do not mature on ~10-Pa vmIPNs under both proliferating and differentiation conditions. Interestingly, cells on surfaces above this threshold experience an optimum in proliferation rate as a function of modulus (Fig. 2 *C*). On laminin-coated polystyrene substrates, phosphoinositide 3-OH kinase (PI3K)/Akt-mediated FGF-2 stimulated aNSC self-renewal (44), and this pathway may intersect with mechanotransducive pathways that are activated on RGD-modified vmIPNs of ≥100 Pa. Interestingly, the mechanical stretch of 3T3 fibroblast cells increased the activation of an important RGD receptor, $\alpha_v\beta_3$ integrin, and was mediated by PI3K/Akt (45). How PI3K/Akt, integrins, and moduli combine to regulate aNSC self-renewal merits future work.

The aNSCs also respond to the vmIPN modulus during cell differentiation. For example, GFAP, a marker of astrocytes, was uniform across vmIPN moduli, but cell number decreased at lower stiffness (Fig. 4), indicating that softer vmIPN moduli selected against astrocytes, but did not affect the extent of differentiation of cells that did differentiate. In addition, β-tubulin III protein levels are known to increase progressively with neuronal differentiation during the early lineage commitment of aNSCs, and thus represent the extent of neuronal maturation (22). Six days after FGF removal and retinoic-acid addition, staining revealed no overall difference in the percentage of β-tubulin III$^+$ cells as a function of substrate moduli (data not shown). However, QRT-PCR and staining both showed that neurons have greater β-tubulin III mRNA and protein levels on vmIPNs of 500–1000 Pa (Fig. 5), indicating that modulus impacts neuronal maturation. Future studies involving pharmacologic inhibitors, genetically modified NSCs, and global gene-expression analysis could probe potential stem-cell signaling and transcriptional networks that respond to stiffness (14,15,46,47).

Under conditions where cells undergo mixed differentiation (serum and retinoic acid), the proportion of neurons progressively decreases and the fraction of astrocytes increases as vmIPN moduli increase (Fig. 6). This intriguing result could be attributable to an instructive role of modulus, where stiffness directly regulates cell-lineage commitment, or a selective role, where cells differentiate into the two lineages to the same extent on each surface, but survival is differentially favored at different stiffnesses. In support of a potential selective role, previous work with mixed rat embryonic (E17–E19) cortical progenitors showed that neuronal cell types engraft onto soft substrates better than glial cell types (21). This interpretation is also consistent with the observation that astrocyte numbers decrease with softer moduli under astrocytic differentiation conditions (Fig. 4). However, the relative roles of instruction versus selection warrant further study. Full knowledge of the regulatory machinery specifying lineage commitment is lacking in aNSCs, but recent work indicated that specific basic-helix-loop-helix transcription factors control lineage commitment and neuronal differentiation in aNSCs (M.J. Robertson and D.V. Schaffer, unpublished data).

Our study used culture systems with physiologically relevant mechanical and biochemical properties, to advance both basic and applied stem-cell biology efforts. Adult NSCs (24,34,39) have different functional roles in vivo than do previously studied cells, including primary late embryonic neural cultures (21,41,48) or early postnatal differentiated neurons (20). Moreover, our study examined cell behavior over a broad range of moduli, spanning native brain tissue, and with a specific well-defined adhesion ligand, the bsp-RGD(15) peptide. Furthermore, we present novel quantitative data on self-renewal as a function of modulus. These results collectively suggest that optimal cell differentiation occurs in physiologically relevant environments. The optimal proliferation rate of dividing cells occurs near the stiffness of the brain ($E' \approx 500$ Pa), and biomedical applications that require scalable stem-cell expansion and differentiation could benefit from using systems whose stiffness matches this modulus. Furthermore, local variation in stiffness could be used as a control parameter to tune cell differentiation in the brain, and stiffness could play a role in central nervous system pathology, including injury homing responses of NSCs to stiff glial scars or areas of hypoxia (49). Finally, this work may provide design principles for tissue-engineering efforts involving injections of materials or materials plus cells into the adult brain or other central nervous system locations. These possibilities merit future investigation.

CONCLUSIONS

Synthetic vmIPN culture substrates with elastic moduli in the range of neural tissue were generated to explore the effects of modulus on adult neural stem-cell self-renewal and differentiation. Importantly, the synthesis procedure maintained a constant, well-defined surface chemistry and peptide ligand density, so that the effects of substrate elastic modulus on stem-cell self-renewal and differentiation could be examined. The results demonstrated that aNSCs can self-renew and differentiate on RGD peptide-modified vmIPNs of ≥100-Pa elastic modulus. In addition, the expression of a neuronal marker after 6 days of neuronal differentiation exhibited an optimum at vmIPNs of $E' \sim 500$ Pa, and astrocyte numbers progressively decreased in softer materials under astrocyte differentiation conditions. Finally, the proportion of neurons versus glia under mixed differentiation is a strong function of modulus. These results demonstrate that tuning the mechanical properties of a synthetic culture substrate offers a means to modulate or control neural stem-cell behavior.

The authors thank R. Hayward, S. Kumar, T. Ulrich, and E. de Juan-Pardo for technical assistance, advice, and discussions.

This work was funded in part by a National Defense Science and Engineering Graduate Fellowship (A.K.), a National Science Foundation fellowship (L.L.), and grant 2005-280 from the Graduate Research and Education in Adaptive Biotechnology Training Program from the University of California Systemwide Biotechnology Research and Education Program (K.S.). Additional support came from Laboratory Directed Research and Development 3668DS.

REFERENCES

1. Bard, J. B., and E. D. Hay. 1975. The behavior of fibroblasts from the developing avian cornea. Morphology and movement in situ and in vitro. *J. Cell Biol.* 67:400–418.
2. Hay, E. D. 1982. Interaction of embryonic surface and cytoskeleton with extracellular matrix. *Am. J. Anat.* 165:1–12.
3. Nakagawa, S., P. Pawelek, and F. Grinnell. 1989. Extracellular matrix organization modulates fibroblast growth and growth factor responsiveness. *Exp. Cell Res.* 182:572–582.
4. Halliday, N. L., and J. J. Tomasek. 1995. Mechanical properties of the extracellular matrix influence fibronectin fibril assembly in vitro. *Exp. Cell Res.* 217:109–117.
5. Pelham, R. J., Jr., and Y. Wang. 1997. Cell locomotion and focal adhesions are regulated by substrate flexibility. *Proc. Natl. Acad. Sci. USA.* 94:13661–13665.
6. Lo, C. M., H. B. Wang, M. Dembo, and Y. L. Wang. 2000. Cell movement is guided by the rigidity of the substrate. *Biophys. J.* 79:144–152.
7. Willits, R. K., and S. L. Skornia. 2004. Effect of collagen gel stiffness on neurite extension. *J. Biomater. Sci. Polym. Ed.* 15:1521–1531.
8. Flanagan, L. A., Y. E. Ju, B. Marg, M. Osterfield, and P. A. Janmey. 2002. Neurite branching on deformable substrates. *Neuroreport.* 13: 2411–2415.
9. Leach, J. B., X. Q. Brown, J. G. Jacot, P. A. Dimilla, and J. Y. Wong. 2007. Neurite outgrowth and branching of PC12 cells on very soft substrates sharply decreases below a threshold of substrate rigidity. *J. Neural Eng.* 4:26–34.
10. Gunn, J. W., S. D. Turner, and B. K. Mann. 2005. Adhesive and mechanical properties of hydrogels influence neurite extension. *J. Biomed. Mater. Res. A.* 72:91–97.
11. Thomas, T. W., and P. A. DiMilla. 2000. Spreading and motility of human glioblastoma cells on sheets of silicone rubber depend on substratum compliance. *Med. Biol. Eng. Comput.* 38:360–370.
12. Wozniak, M. A., R. Desai, P. A. Solski, C. J. Der, and P. J. Keely. 2003. ROCK-generated contractility regulates breast epithelial cell differentiation in response to the physical properties of a three-dimensional collagen matrix. *J. Cell Biol.* 163:583–595.
13. Engler, A. J., M. A. Griffin, S. Sen, C. G. Bonnemann, H. L. Sweeney, and D. E. Discher. 2004. Myotubes differentiate optimally on substrates with tissue-like stiffness: pathological implications for soft or stiff microenvironments. *J. Cell Biol.* 166:877–887.
14. McBeath, R., D. M. Pirone, C. M. Nelson, K. Bhadriraju, and C. S. Chen. 2004. Cell shape, cytoskeletal tension, and RhoA regulate stem cell lineage commitment. *Dev. Cell.* 6:483–495.
15. Engler, A. J., S. Sen, H. L. Sweeney, and D. E. Discher. 2006. Matrix elasticity directs stem cell lineage specification. *Cell.* 126:677–689.
16. Elkin, B. S., E. U. Azeloglu, K. D. Costa, and B. Morrison III. 2007. Mechanical heterogeneity of the rat hippocampus measured by atomic force microscope indentation. *J. Neurotrauma.* 24:812–822.
17. Lu, Y. B., K. Franze, G. Seifert, C. Steinhauser, F. Kirchhoff, H. Wolburg, J. Guck, P. Janmey, E. Q. Wei, J. Kas, and others. 2006. Viscoelastic properties of individual glial cells and neurons in the CNS. *Proc. Natl. Acad. Sci. USA.* 103:17759–17764.
18. Discher, D. E., P. Janmey, and Y. L. Wang. 2005. Tissue cells feel and respond to the stiffness of their substrate. *Science.* 310:1139–1143.
19. Diridollou, S., F. Patat, F. Gens, L. Vaillant, D. Black, J. M. Lagarde, Y. Gall, and M. Berson. 2000. In vivo model of the mechanical properties of the human skin under suction. *Skin Res. Technol.* 6:214–221.
20. Kostic, A., J. Sap, and M. P. Sheetz. 2007. RPTP$\{\alpha\}$ is required for rigidity-dependent inhibition of extension and differentiation of hippocampal neurons. *J. Cell Sci.* 120:3895–3904.
21. Georges, P. C., W. J. Miller, D. F. Meaney, E. S. Sawyer, and P. A. Janmey. 2006. Matrices with compliance comparable to that of brain tissue select neuronal over glial growth in mixed cortical cultures. *Biophys. J.* 90:3012–3018.
22. Gage, F. H. 2000. Mammalian neural stem cells. *Science.* 287:1433–1438.
23. Rakic, P. 1985. Limits of neurogenesis in primates. *Science.* 227:1054–1056.
24. Palmer, T. D., J. Ray, and F. H. Gage. 1995. FGF-2-responsive neuronal progenitors reside in proliferative and quiescent regions of the adult rodent brain. *Mol. Cell. Neurosci.* 6:474–486.
25. Zhang, C. L., Y. Zou, W. He, F. H. Gage, and R. M. Evans. 2008. A role for adult TLX-positive neural stem cells in learning and behaviour. *Nature.* 451:1004–1007.
26. Robertson, M. J., P. Gip, and D. V. Schaffer. 2008. Neural stem cell engineering: directed differentiation of adult and embryonic stem cells into neurons. *Front. Biosci.* 13:21–50.
27. Schaffer, D. V., A. O'Neill, L. Hochrein, and T. McGranahan. 2004. Quantitative analysis of signaling mechanisms controlling adult neural progenitor cell proliferation. *Conf. Proc. IEEE Eng. Med. Biol. Soc.* 7:4965.
28. Gefen, A., and S. S. Margulies. 2004. Are in vivo and in situ brain tissues mechanically similar? *J. Biomech.* 37:1339–1352.
29. Saha, K., E. F. Irwin, J. Kozhukh, D. V. Schaffer, and K. E. Healy. 2007. Biomimetic interfacial interpenetrating polymer networks control neural stem cell behavior. *J. Biomed. Mater. Res. A.* 81:240–249.
30. Harbers, G. M., L. J. Gamble, E. F. Irwin, D. G. Castner, and K. E. Healy. 2005. Development and characterization of a high-throughput system for assessing cell-surface receptor-ligand engagement. *Langmuir.* 21:8374–8384.
31. Harbers, G. M., and K. E. Healy. 2005. The effect of ligand type and density on osteoblast adhesion, proliferation, and matrix mineralization. *J. Biomed. Mater. Res. A.* 75:855–869.
32. Bearinger, J. P., D. G. Castner, and K. E. Healy. 1998. Biomolecular modification of p(AAm-co-EG/AA) IPNs supports osteoblast adhesion and phenotypic expression. *J. Biomater. Sci. Polym. Ed.* 9:629–652.

33. Irwin, E. F., J. E. Ho, S. R. Kane, and K. E. Healy. 2005. Analysis of interpenetrating polymer networks via quartz crystal microbalance with dissipation monitoring. *Langmuir*. 21:5529–5536.

34. Lai, K., B. K. Kaspar, F. H. Gage, and D. V. Schaffer. 2003. Sonic hedgehog regulates adult neural progenitor proliferation in vitro and in vivo. *Nat. Neurosci*. 6:21–27.

35. Irwin, E. F., K. Saha, M. Rosenbluth, L. J. Gamble, D. G. Castner, and K. E. Healy. 2008. Modulus-dependent macrophage adhesion and behavior. *J. Biomater. Sci. Polym. Ed*. In press.

36. Miyake, K., N. Satomi, and S. Sasaki. 2006. Elastic modulus of polystyrene film from near surface to bulk measured by nanoindentation using atomic force microscopy. *Appl. Phys. Lett*. 86:031925-1–031925-3.

37. Abranches, E., A. O'Neill, M. J. Robertson, D. V. Schaffer, and J. M. Cabral. 2006. Development of quantitative PCR methods to analyse neural progenitor cell culture state. *Biotechnol. Appl. Biochem*. 44:1–8.

38. Lamprecht, M. R., D. M. Sabatini, and A. E. Carpenter. 2007. CellProfiler: free, versatile software for automated biological image analysis. *Biotechniques*. 42:71–75.

39. Suh, H., A. Consiglio, J. Ray, T. Sawai, K. A. D'Amour, and F. H. Gage. 2007. In vivo fate analysis reveals the multipotent and self-renewal capacities of Sox2(+) neural stem cells in the adult hippocampus. *Cell Stem Cell*. 1:515–528.

40. Takahashi, J., T. D. Palmer, and F. H. Gage. 1999. Retinoic acid and neurotrophins collaborate to regulate neurogenesis in adult-derived neural stem cell cultures. *J. Neurobiol*. 38:65–81.

41. Soen, Y., A. Mori, T. D. Palmer, and P. O. Brown. 2006. Exploring the regulation of human neural precursor cell differentiation using arrays of signaling microenvironments. *Mol. Syst. Biol*. 2:37.

42. Saha, K., J. F. Pollock, D. V. Schaffer, and K. E. Healy. 2007. Designing synthetic materials to control stem cell phenotype. *Curr. Opin. Chem. Biol*. 11:381–387.

43. Yeung, T., P. C. Georges, L. A. Flanagan, B. Marg, M. Ortiz, M. Funaki, N. Zahir, W. Ming, V. Weaver, and P. A. Janmey. 2005. Effects of substrate stiffness on cell morphology, cytoskeletal structure, and adhesion. *Cell Motil. Cytoskeleton*. 60:24–34.

44. Peltier, J., A. O'Neill, and D. V. Schaffer. 2007. PI3K/Akt and CREB regulate adult neural hippocampal progenitor proliferation and differentiation. *Developmental Neurobiology*. 67:1348–1361.

45. Katsumi, A., T. Naoe, T. Matsushita, K. Kaibuchi, and M. A. Schwartz. 2005. Integrin activation and matrix binding mediate cellular responses to mechanical stretch. *J. Biol. Chem*. 280:16546–16549.

46. Chen, T. J., S. Gehler, A. E. Shaw, J. R. Bamburg, and P. C. Letourneau. 2006. Cdc42 participates in the regulation of ADF/cofilin and retinal growth cone filopodia by brain derived neurotrophic factor. *J. Neurobiol*. 66:103–114.

47. Gualdoni, S., C. Albertinazzi, S. Corbetta, F. Valtorta, and I. de Curtis. 2007. Normal levels of Rac1 are important for dendritic but not axonal development in hippocampal neurons. *Biol. Cell*. 99:455–464.

48. Silva, G. A., C. Czeisler, K. L. Niece, E. Beniash, D. A. Harrington, J. A. Kessler, and S. I. Stupp. 2004. Selective differentiation of neural progenitor cells by high-epitope density nanofibers. *Science*. 303: 1352–1355.

49. Imitola, J., K. Raddassi, K. I. Park, F. J. Mueller, M. Nieto, Y. D. Teng, D. Frenkel, J. Li, R. L. Sidman, C. A. Walsh, and others. 2004. Directed migration of neural stem cells to sites of CNS injury by the stromal cell-derived factor 1alpha/CXC chemokine receptor 4 pathway. *Proc. Natl. Acad. Sci. USA*. 101:18117–18122.